Elsevier Editorial System(tm) for Colloids and Surfaces B: Biointerfaces
Manuscript Draft

Manuscript Number: COLSUB-D-14-01450R1

Title: Biofunctionalization of REDV elastin-like recombinamers improves endothelialization on CoCr alloy surfaces for cardiovascular applications

Article Type: Full Length Article

Keywords: CoCr alloy, Surface functionalization, Elastin-like recombinamers, Biomimetic materials, Endothelialization

Corresponding Author: Dr. Marta Pegueroles,

Corresponding Author's Institution: Technical University of Catalonia

First Author: Maria Isabel Castellanos

Order of Authors: Maria Isabel Castellanos; Anne-Sophie Zenses; Anna Grau; Jose Carlos Rodríguez-Cabello; Francisco Javier Gil; José María Manero; Marta Pegueroles

Manuscript Region of Origin: SPAIN

Abstract: To improve cardiovascular implant success, metal-based stents are designated to modulate endothelial cells adhesion and migration in order to prevent restenosis and late thrombosis diseases. Biomimetic coatings with extra-cellular matrix adhesive biomolecules onto stents surfaces are a strategy to recover a healthy endothelium. However, the appropriate bioactive sequences to selective promote growth of endothelium and the biomolecules surface immobilization strategy remains to be elucidated. In this study, biofunctionalization of cobalt chromium, CoCr, alloy surfaces with elastin-like recombinamers, ELR, genetically modified with an REDV sequence, was performed to enhance metal surfaces endothelialization. Moreover, physical adsorption and covalent bonding were used as biomolecules binding strategies onto CoCr alloy. Surfaces were activated with plasma and etched with sodium hydroxide previous to silanization with 3-chloropropyltriethoxysilane and functionalized with the ELR. CoCr alloy surfaces were successfully biofunctionalized and the use of an ELR with an REDV sequence, allows conferring bioactivity to the biomaterials surface, demonstrating a higher cell adhesion and spreading of HUVEC cells on the different CoCr surfaces. This effect is emphasized as increases the amount of immobilized biomolecules and directly related to the immobilization technique, covalent bonding, and the increase of surface charge electronegativity. Our strategy of REDV elastin-like recombinamers immobilization onto CoCr alloy surfaces via covalent bonding through organosilanes provides a bioactive surface that promotes endothelial cell adhesion and spreading.

Response to Reviewers: Responses to reviewer’s comments:

We are grateful to reviewers for the critical comments and useful suggestions that have helped us to improve our paper. As indicated in the responses that follow, we have taken all these comments and suggestions into account in the revised version of our paper. Answers to the Reviewers’ comments are written in blue. The main text is revised according to these answers and written in red.

To reviewer #1

***Graphical Abstract (for review)**

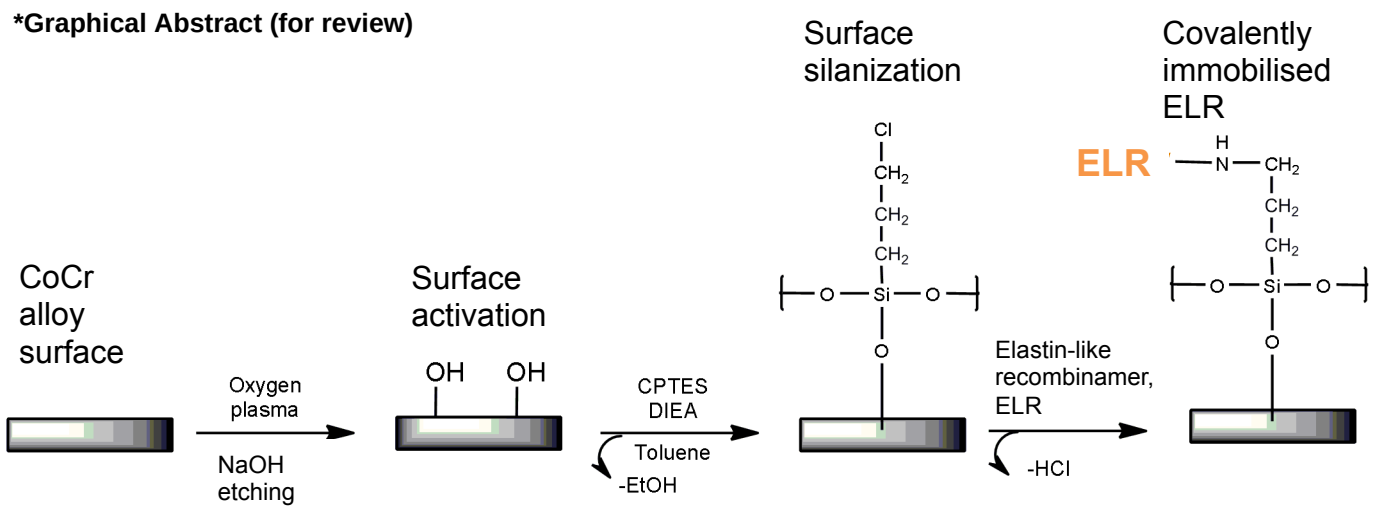

Highlights

- We immobilized an elastin-like recombinamer, ELR, on CoCr, alloy through physisorption and covalent bonding.
- The ELR combines a bioactive motif specific for endothelial cell adhesion.
- The ELR immobilization is enhanced with silanization and surface charge.
- The ELR coated surfaces displayed an improved HUVEC cell adhesion and spreading.

Title: **Biofunctionalization of REDV elastin-like recombinamers improves endothelialization on CoCr alloy surfaces for cardiovascular applications**

Authors: Maria Isabel Castellanos[1,2,3], Anne-Sophie Zenses[1,3], Anna Grau[1,3], Jose Carlos Rodríguez-Cabello[2,4], Francisco Javier Gil[1,2,3], Jose María Manero[1,2,3], Marta Pegueroles[1,2,3,*].

Affiliations: [1] Biomaterials, Biomechanics and Tissue Engineering Group, Department of Materials Science and Metallurgy, Technical University of Catalonia (UPC), Av. Diagonal 647, 08028 Barcelona, Spain
[2] Biomedical Research Networking Centre in Bioengineering, Biomaterials and Nanomedicine (CIBER-BBN), Maria de Luna 11, Ed. CEEI, 50118 Zaragoza, Spain
[3] Centre for Research in NanoEngineering (CRNE), UPC, C/Pascual i Vila 15, 08028 Barcelona, Spain
[4] GIR BIOFORGE (Group for Advanced Materials and Nanobiotechnology), Universidad de Valladolid (UVA), Valladolid 47011, Spain.

Corr. Author: * Marta Pegueroles, PhD
marta.pegueroles@upc.edu
Biomaterials, Biomechanics and Tissue Engineering Group
Department of Materials Science and Metallurgy
Technical University of Catalonia (UPC)
Av. Diagonal 647
08028 Barcelona
Spain.
Tel: +34 934054154
Fax: +34 934016706

Maria Isabel Castellanos: maria.isabel.castellanos@upc.edu
Anne-Sophie Zenses: annesophie.zenses@gmail.com
Anna Grau: agraugar@gmail.com
Jose Carlos Rodríguez-Cabello: cabello@bioforge.uva.es
Francisco Javier Gil: francesc.xavier.gil@upc.edu
Jose María Manero: jose.maria.manero@upc.edu
Marta Pegueroles: marta.pegueroles@upc.edu

Abstract

To improve cardiovascular implant success, metal-based stents are designated to modulate endothelial cells adhesion and migration in order to prevent restenosis and late thrombosis diseases. Biomimetic coatings with extra-cellular matrix adhesive biomolecules onto stents surfaces are a strategy to recover a healthy endothelium. However, the appropriate bioactive sequences to selective promote growth of endothelium and the biomolecules surface immobilization strategy remains to be elucidated. In this study, biofunctionalization of cobalt chromium, CoCr, alloy surfaces with elastin-like recombinamers, ELR, genetically modified with an REDV sequence, was performed to enhance metal surfaces endothelialization. Moreover, physical adsorption and covalent bonding were used as biomolecules binding strategies onto CoCr alloy. Surfaces were activated with plasma and etched with sodium hydroxide previous to silanization with 3-chloropropyltriethoxysilane and functionalized with the ELR. CoCr alloy surfaces were successfully biofunctionalized and the use of an ELR with an REDV sequence, allows conferring bioactivity to the biomaterials surface, demonstrating a higher cell adhesion and spreading of HUVEC cells on the different CoCr surfaces. This effect is emphasized as increases the amount of immobilized biomolecules and directly related to the immobilization technique, covalent bonding, and the increase of surface charge electronegativity. Our strategy of REDV elastin-like recombinamers immobilization onto CoCr alloy surfaces via covalent bonding through organosilanes provides a bioactive surface that promotes endothelial cell adhesion and spreading.

Keywords

CoCr alloy; Surface functionalization; Elastin-like recombinamers; Biomimetic materials; Endothelialization.

1. Introduction

Coronary angioplasty and stent insertion is the major surgery to solve cardiovascular disease [1,2]. However, in-stent restenosis (ISR), stents thrombosis (ST) and incomplete stent endothelialization remain the principal mechanisms for the failure of the bare-metal stents (BMS) and drug-eluting stents (DES) after implantation [3]. Interestingly, ISR, is developed in 20%-30% of lesions treated with BMS and in <10% when treated with DES. ISR consists of artery narrowing within the stented segment due to neointimal hyperplastia and over-proliferation of vascular smooth muscle cells (SMCs) [4–6]. Despite the decrease in the ISR rate, DES, delays the formation of healthy endothelium due to the delivery of antiproliferative drugs and suffers from late ST increasing the patients time anti-platelet therapy [7]. The native and healthy endothelium is an active organ that maintains vessel integrity and modulates vascular tone, consisting of a monolayer of endothelial cells, thereby reducing the potential for thrombosis and restenosis. Several studies have demonstrated that stent surface endothelialization is a well-known methodology to inhibit the restenosis and thrombosis [7–9].

Control of cell-material interactions, and thus cell behaviour, may first be achieved by preventing nonspecific protein adsorption and undesirable cell adhesion and, second, by exposing specific cell ligands or bioactive molecules to optimize the adhesion, migration and/or proliferation of desired cells. Biofunctionalization with cell adhesive molecules onto metallic surfaces is a well-established process to control and guide cellular response [10,11]. Different biomolecules are used such as the immobilization of extracellular matrix (ECM) proteins, where the maintenance of the native form enhances their biological function but they present immunological problems, they are difficult to purify and to control their functionalization [6,12]. Another strategy is the use of short peptides, which are non-immunogenic and easy to control their surface immobilization, but, they cannot carry on some functionalities that natural proteins can [13,14]. The use of recombinant proteins such as elastin like-elastin recombinamers (ELR) can avoid the mentioned problems and highlight the indicated advantages. ELR are oligomeric macromolecules based on the repetition of the (VPGXG) motif from elastin, in which X is any amino acid except L-proline [15]. The composition is strictly defined by engineering design and enable the introduction of peptide sequences to extend their properties, they are produced as recombinant proteins mimicking the basic properties of elastin and exhibiting mono-dispersity and a high control over amino acid sequence [16,17]. The recombinant nature of ELRs allows to include bioactive domains such as endothelial cell attachment sequence arginine–(glutamic acid)– (aspartic acid)–valine (REDV) [7,16], which mediates endothelial cell adhesion and spreading on fibronectin via its $\alpha_4\beta_1$ receptor [18,19] over smooth muscle cells and platelets [20].

CoCr alloy is a biocompatible material widely used as in coronary stents due to its non-toxicity, elasticity, plasticity, corrosion resistance addition to maintaining the radiopacity and radial strength [21,22]. However, these materials are bioinert, thus leading in some cases to long endothelialization processes that can be overcome with biochemical surface modification through the immobilization of an ELR with an REDV sequence [7,10,11] onto metallic stents surface.

Immobilization of cell adhesive motifs onto metallic surfaces can be enhanced by the surface activation through physicochemical surface modification to promote a physical adsorption and/or covalent bonding. Surface properties such as surface hydrophilicity/hydrophobicity, roughness, texture, chemical composition, electrical charge and morphology play an important role on surface functionalization and then, on cell response [23].

The aim of the present work was to obtain a new family of biofunctionalized CoCr alloy surfaces with REDV elastin-like recombinamers using two different surface activation treatments (plasma and NaOH etching) and two anchoring mechanisms (physisorption and covalent immobilization), and evaluate the immobilized ELR and the in vitro HUVEC cell adhesion response.

2. Materials and Methods

2.1 Materials

2.1.1 Metallic surfaces

CoCr alloy (Co-20Cr-14.6W-10.8Ni-2.5Fe-1.5Mn, ASTM F90) (Technalloy Company) discs of 8,5 mm diameter and 2 mm thick were abraded subsequently with 240, 400, 600, 800 and 1200 grit silicon carbide abrasive paper and finally polished with a water suspension of 1 μm and 0.05 μm alumina powder. Prior to the surface treatments, all samples were ultrasonically cleaned with ethanol, distilled water and acetone for 5 min each.

2.1.2 Elastin-like recombinamers (ELRs)

Elastin-like recombinamers (ELRs) were provided and synthesized by the BIOFORGE group at the University of Valladolid, Spain. The elastin-like recombinamers are governed by $(VPGXG)_n$ module in which X is any amino acid except L-proline and that include other amino-acidic sequences following already optimized protocols [15–17]. ELR with an REDV sequence, Arg-Glu-Asp-Val, for endothelial cell adhesion was designed with the following sequence [17]:

REDV: $((VPGIG)_2(VPGKG)(VPGIG)_2EEQIGHIP\mathbf{REDV}DYHLYP(VPGIG)_2(VPGKG)(VPGIG)_2(VGVAPG)_3)_{10}$

2.1.3 Cells

Human umbilical vein endothelial cells, HUVEC´s (Lonza Group Ldt, Basel, Switzerland,) were grown in endothelial cell basal medium (EBM®) medium, with 5% FBS, 0.1% GA-100, 0.1% rhEGF (growth factor), 0.4% BBE and 0.1% Hydrocortisone (Lonza, Cologne, Germany) at 37°C in a 5% CO_2/ 95% air atmosphere and at 100% humidity. The culture medium was changed every 2 days. For the experiments, cell culture flasks Nunc, (Thermo Scientific, Roskilde, Denmark) were pre-coated with 1μg/ml fibronectin solution in PBS 1X, FN, and cells were harvested at 70–90% confluence by trypsin/EDTA (Sigma-Aldrich, Missouri, United States), centrifuged and re-suspended in a serum-free medium before being plated at 2 x 10^4 HUVEC cells per sample.

HUVEC cell passage between 4 and 8 was used for all the experiments [24,25].

2.2 Surface functionalization

Bioactivity of the polished CoCr surfaces (**CT**) was achieved by means of ELRs covalent functionalization through the following steps: (1) surface activation, (2) silanization and (3) immobilization of ELRs. First, the surface activation treatments applied to the samples were as follows:

PL: Oxygen plasma surface treatment with a Plasma Cleaner (Sterilizer PDC-002, Harrick Scientific Corporation, United States) for 5 min at high power setting.

NA: Basic etching with 5 M NaOH solution during 2 h at RT. Next, samples were cleaned twice in distilled water during 30 min.

Then, as a second step, each of the previous series were silanized immediately by immersing the substrate in a solution of 10 ml of anhydrous toluene, 1 ml (0.05 M) of N,N - diisopropylethylamine (DIEA) and 2 ml (0.5 M) of 3-chloropropyltriethoxysilane (CPTES) (Sigma-Aldrich, Missouri, United States) per disk under nitrogen atmosphere for 1 h at 90 °C under stirring. The nomenclature used throughout the text for control, plasma and sodium hydroxide treated surfaces silanized with CPTES was CT-CP, PL-CP and NA-CP, respectively. After reaction, the discs were ultrasonically rinsed with cyclohexane, isopropanol, distilled water, and acetone, for 15 min each and were finally dried with nitrogen. The CPTES-modified substrates were stored under vacuum in argon atmosphere.

Finally, ELR was immobilised on the CoCr surface by two different methods: (1) physical adsorption on the control, plasma and sodium hydroxide treated surfaces (the samples were coded as CT-REDV, PL-REDV, NA-REDV); and (2) covalent immobilisation through a CPTES silanization process of the previously control, plasma and sodium hydroxide treated surfaces (the samples were coded CT-CP-REDV, PL-CP-REDV, NA-CP-REDV). Activated and silanized samples were incubated overnight at room temperature and at a biopolymer concentration of 500 μg/ml of

dissolved elastin-like recombinamers with an REDV sequence in ultrapure Milli-Q water and the pH adjusted to 13.0 with Na_2CO_3 O/N at RT to ensure that all the amines were deprotonated to facilitate nucleophilic attack. Afterwards, the solution was removed and samples thoroughly washed with water and dried in a stream of nitrogen and immediately analyzed as described below.

In summary, the following groups of surfaces were studied: a) CoCr surfaces (CT, PL, NA); b) CPTES grafted surfaces (CT-CP, PL-CP, NA-CP); c) elastin-like recombinamer physisorbed surfaces (CT-REDV, PL-REDV, NA-REDV) and; d) elastin-like recombinamer silanized surfaces (CT-CP-REDV, PL-CP-REDV, NA-CP-REDV).

2.3 Surface characterization

2.3.1 Surface roughness

Surface roughness measurements were performed with white light interferometry (Optical interferometer VeecoWyko 9300NT, Veeco Instruments, USA). Type of measurement VSI (Vertical Scanning Interferometry). Three samples of each treatment series were analysed and three measurements of roughness were carried out. Data analysis was performed with Wyko Vision 4.10 software (Veeco Instruments). Curvature and tilt were eliminated from every surface analysis with a Gaussian filter. The average roughness (Ra), arithmetic average of the absolute values of the profile height deviations from the mean plane, and the surface index area (SIA), ratio between real and nominal area, were quantified from the topographical images.

2.3.2 Wettability and surface free energy

The wettability studies were performed using the sessile drop method with a contact angle video based system (Contact Angle System OCA15plus, Dataphysics, Germany) and analysed with the SCA20 software (Dataphysics, Germany). For each measure, 3 µl of distilled water (miliQ) and 3 µl of diiodomethane were used [26]. Contact angles for SFE calculations were measured at room temperature and the drop deposited on the surface after the same cleaning procedures and treatments.

For each sample, fifteen drops were analysed. The surface free energies (SFE) of the different treatments were calculated using the Owens and Wendt approach (OW) adaptation of Young´s equation [27,28]:

$$\gamma_s = \gamma_s^d + \gamma_s^p \quad (1)$$

$$\gamma_l.(1+\cos\theta) = 2.(\gamma_l^d.\gamma_s^d)^{1/2} + 2.(\gamma_l^p.\gamma_s^p)^{1/2} \quad (2)$$

where γ_l^d is the dispersive part of liquid surface tension, γ_s^d is the dispersive part of the solid SFE, γ_l^p is the polar part of liquid surface tension and γ_s^p is the polar part of the solid SFE.

2.3.3 Surface chemical characterization

The chemical analysis of the surface, before and after activation, silanization procedures and ELRs attachment, was investigated by X-ray photoelectron spectroscopy (XPS) (SPECS Surface Nano Analysis GmbH, Berlin, Germany), equipped with an Al anode XR50 source operating at 150 W and a Phoibos 150 MCD-9 detector.

The elements present on the surface were qualitatively evaluated by low-resolution survey spectra, whereas high-resolution of some determined elements (C 1s, N 1s, O 1s, Cr 2p, Co 2p, Si 2s, Cl 2p) were recorded with pass energy of 35 eV at 0,1 eV steps at a pressure below $5x10^{-9}$ mbar. The positions of the peaks were referred to the C 1s signal at 284.8 eV. CasaXPS spectrum software (Casa Software Ltd., UK); was used to analyse the different spectra and perform the XPS peak deconvolution of survey and high resolution. Two samples were studied for each surface condition.

2.3.4 Surface Charge

A streaming potential instrument (Surpass Electrokinetic Analyzer, Anton Paar, Austria) with an adjustable gap cell was used to determine apparent ζ-potential of the activated, silanized and functionalized surfaces. The 'titration unit' allows automatically performed series of measurements at a varied-pH solution. A 1 mM KCl solution was used as electrolyte. The pressure ramp was run up to a maximum pressure of 500 mbar. The electrolyte solution was adjusted to a starting pH = 9.0 using 0.1M KOH. The automatic titration was performed down to pH=3.0 adding 0.1 M HCl.

Through the VisioLab software (Anton Paar, Austria), it was determined the value of the isoelectric point (IEP) and the surface charge at pH 7.4. For each surface condition, three measurements were performed.

2.4 ELRs biofunctionalized adlayer characterization

The quantification and characterization of the attached elastin like recombinamers layer were characterized by atomic force microscopy (AFM), FITC fluorescence quantification, XPS analysis and quartz-crystal microbalance with monitoring dissipation (QCM-D).

Topographical changes due to ELR's adsorption onto the different treated surfaces were analyzed using AFM (Multimode, NanoScope V Controller, Veeco, Digital Instruments, USA) associated with the software WSxM, in tapping mode using silicon cantilevers under ambient conditions.

2.4.1 FITC–ELR preparation and adsorption quantification

FITC-labelled REDV elastin-like recombinamer solution (FITC-REDV) 1 ml of 1 mg/ml, has been prepared following the Pierce® FITC Labelling Kit (Thermo Fisher Scientific, USA). The final protein concentration was estimated by measuring the absorbance at 280 nm and 494 nm (UV Mini 1240 spectrophotometer, Shimadzu), and the protein was then stored at 4 ºC.

500 µg/ml FITC-labelled REDV was adsorbed on the different CoCr treated series during overnight at room temperature. Stability tests were performed on physisorbed and silanized surfaces by adsorbing FITC-REDV on the different treated surfaces and then, sonication in PBS 1X during 1 h. The samples were then rinsed three times with PBS 1X. The adsorbed FITC-labelled protein was eluted with 500 µl of 0.2 M NaOH for 2h. The fluorescent intensity of the extracts was measured with a spectrofluorophotometer (Infinite M200 Pro, Tecan, Switzerland). The excitation and emission wavelengths were set at 488 and 530 nm, respectively. Fluorescent measurements of the attached ELR have been performed prior and after sonication.

2.4.2 Quartz crystal microbalance with monitoring dissipation (QCM-D)

A quartz crystal microbalance consists of a piezoelectric quartz crystal sensor that is excited to oscillation at its fundamental resonant frequency, f. The equipment is used to measure very small masses added on the surface of the sensor because an increase in mass (Δm) bound to the quartz surface causes the crystal oscillation frequency to decrease, obtaining a negative shift of the resonance frequency (-Δf). The Sauerbrey relation concludes that the change in resonance frequency is proportional to the change in the adsorbed mass if the adsorbed layer is much smaller than the mass of the crystal [29]. The Voigt model settles for a viscoelastic or thick layer for which Δf is not directly proportional to Δm, i.e. the effectively coupled mass depends on how the oscillatory motion of the crystal propagates into and through the viscoelastic adlayer [30]. In addition to that, most surface-adsorbed protein layers are hydrated, so they are not only highly viscous and cause significant energy dissipation, but also add mass to the adsorbed protein layer. In those cases the dissipation factor, D, simultaneously calculated with f when using the QCM must also be taken into consideration.. The dissipation factor is inversely proportional to the Q-factor of the oscillator [30], which is a nondimensional parameter that compares the time constant for decay of an oscillating physical system's amplitude to its oscillation period as defined by:

Equation 1

$$D = \frac{1}{Q} = \frac{E_{dissipated}}{2 \cdot \pi \cdot E_{stored}}$$

where $E_{dissipated}$ is the energy dissipated during one period of oscillation, and E_{stored} is the energy stored in the oscillating system.

Co-20Cr-15W-10Ni-1.5Mn (QSX999) sensors were purchased at Q-Sense (Sweden). The fundamental mode of the sensors was at 4.95 MHz. Prior to use, the sensors were cleaned as follows: (1) 10 min sonication with ethanol (96 %, Panreac); (2) 10 min sonication with acetone (99.5 %, Panreac); (3) 10 min sonication with MilliQ ultrapure water; and (4) 10 min UV/ ozone chamber (BioForce Nanosciences, Ames, USA). The QCM-D (D300, Q-Sense, Sweden)

measurements were performed at 25ºC by monitoring changes in frequency, Δf (Hz), and dissipation, ΔD ($\times 10^{-6}$), in real-time using Qsoft software (Q-Sense). All raw data was analyzed using QTools software (Q-Sense). Frequency and dissipation curves were fitted to a Voigt viscoelastic model to yield relevant mass, thickness, and kinetic information. The description of the Voigt model and details on its implementation using a QCM-D are reported elsewhere [30].

Monitoring the adsorption was conducted as follows. The baseline was completely stabilized with PBS 1X for 30-60 min, 500 µg/ml REDV was introduced and maintained in the sensor chamber for 120 min, and the biomolecules weakly bound to the surface were rinsed with PBS 1X for 10 min.

2.5 *In vitro* cell adhesion and proliferation studies

Prior to cell adhesion and proliferation assays functionalized samples were blocked for 1 h at 37 ºC with 5% bovine serum albumin, BSA, in PBS 1X. HUVEC cell adhesion and morphology, after 4 h cell culture with serum-free medium, were evaluated by fluorescence with fluorescein diacetate (FDA) staining which was added directly to the medium to give a final concentration of 1 µg/ml (from a stock of 1 mg/ml in acetone) for 3 min. The stained living cells, the only ones able to convert the dye to a fluorescent analogue, were viewed and photographed with an inverted fluorescent microscope (Upright Microscope Nikon E1000, Japan). All cellular studies were done using triplicates and repeat at least in two independent assays to ensure reproducibility.

The microscope settings were kept constant allowing comparative measurements at several points on the surface. Different cell morphology parameters were studied by ImageJ software: cells per cm^2, total surface area occupied by cells (%), aspect ratio (maximum ratio of width and height of a bounding rectangle for the cell) and maximum diameter (maximum cell length).

HUVEC cells were seeded on the tested surfaces and incubated for 4 h in serum-free medium. Then, the medium was replaced with serum containing one (2% FBS) and the cells were cultured for 1 and 3 days. Untretated CoCr discs (CT) were used as control. Cell number was evaluated by lactate dehydrogenase (LDH) assay. For that purpose, the samples were washed twice with PBS to remove unattached cells, and lysed by addition of Mammalian Protein Extraction Reagent (M-PER), Thermo Scientific, Germany). LDH activity was determined spectrophotometrially with a commercially available LDH kit (Roche, Germany) in a plate reader (Power WaveX, Bio-Tek Instruments, USA; 490 nm). A calibration curve with decreasing numbers of cells was calculated. Results were normalized vs their corresponding surface area (cell /cm^2).

2.6 Statistical analysis

All experiments data presented in this study are given as mean values ± standard deviations.

For the statistical study of the obtained results a non-parametric Mann-Whitney U-test test was used to determine statistically significant differences (p-value < 0.05) between the different groups. Statistical analysis was performed using Minitab software (Minitab Inc, United States).

3. Results

3.1 Surface characterization

3.1.1 Surface roughness

Activation methods slightly affected surface roughness as determined by white light interferometry. Sodium hydroxide etching created a higher roughness (16.0 ± 2.8 nm) while plasma treatment (4.5 ± 0.5 nm) obtained the lowest Ra value compared to control (6.3 ± 2.3 nm). Moreover, any activation treatment affected the surface area of control samples obtaining a SIA value of 1.0 for all the studied surfaces.

3.1.2 Wettability and surface free energy

Wettability results of the treated and silanized CoCr surfaces are shown in Fig. 1, where water contact angles, CA,

and SFE are described. Activation treatments affected wettability behaviour of CoCr surfaces, while NA etching induced a slightly increase of the CA, plasma treatment exhibited the highest hydrophilic behaviour among the others surfaces. This enhancement was accompanied by a slightly decrease of the polar part for NA series, and a statistically significant increase of such component, and total SFE, in PL series compared to control.

Silanization process slightly decreased contact angle values of CT-CP and NA-CP series. Otherwise, plasma treated surfaces presented a significant increment of the contact angle after silanization, PL-CP (from ~19.1^0 up to 76.7^0).

As shown in Fig. 1b, the process of silanization induces changes in SFE mainly due to variations in its polar part. Two effects were noticeable: while the polar component considerably decreased for the PL treated surfaces (from 31.7 to 5.80 mJ/m^2), it slightly increased for CT-CP and NA-CP, whereas dispersive component of CT-CP, PL-CP and NA-CP were statistically equal.

3.1.3 Surface chemical characterization

XPS analysis was performed to examine the atomic ratios of the most significant elements (C, O, N, Co, Cr, Ni, W, Cl, Si) of the CoCr alloy surfaces with different surface qualities (Table 1).

The activation of CoCr surfaces with plasma, PL, decreased the percentage of carbon and nitrogen and increased the amount of oxygen compared to control, CT. Contrary, NaOH etching activation slightly decreased carbon content and increased the amount oxygen and nitrogen.

To further characterize the activation process on CoCr surfaces, high-resolution C 1s (Fig. 2a) and O 1s (Fig. 2b) XPS spectra were studied. Deconvolution of C 1s peak, detected a major peak at 284.5 eV, assigned to aliphatic carbon [31,32] on CT, PL and NA surfaces. Three more peaks were observed at different binding energies. A peak at 282.7 eV, is attributed to chromium carbide [33], while at 285.6 eV, it is attributed to oxygen-containing hydrocarbon fragment C-OH [32]. Finally at 288.1 eV, indicates the presence of C=O polar compounds on the surface [34]. The analysis of the O 1s peak, Fig. 2b, revealed three contributions: 529.5 eV is assigned to metal oxide (O^{2-}) species [35–37], 531.3 eV corresponds to hydroxyls (-OH) species and at 532.8 eV is assigned to H_2O groups [34].

The activation treatments increased the intensity of the hydroxyl group signal, 531.3 eV, and deceased the intensity signal of oxides and H_2O groups compared to CT surfaces, especially high is for PL activated surfaces (Fig. 2b). Moreover, the ratio OH^-/O^{2-} was of 1.32 for CT samples, 8.63 for PL and 1.62 for NA confirming the important activation behaviour of plasma treatment on CoCr alloys compared to CT and NA.

The silanization of CoCr samples was characterized by the presence of Cl 2p and Si 2s at the CT-CP, PL-CP and NA-CP samples (Table 1) compared to activated series where any trace of these components was detected.

XPS studies confirmed the attachment of REDV through covalent functionalization or physisorption resulting in a significant increase of the percentage of C 1s and N 1s and reductions of the intensity of O 1s, Co 2p and Cr 2p (CT-REDV, PL-REDV, NA-REDV, CT-CP-REDV, PL-CP-REDV, NA-CP-REDV) in comparison with activated surfaces (CT, PL, NA) (Table 1). Additionally, REDV functionalized surfaces significantly increased the signal intensity of the C 1s sub peak at 288.1 eV (Fig. 2a), attributed to amide groups (N-C=O) and also overlaps with C=O polar compounds, compared to control and activated surfaces (CT: 8.25%, CT-REDV: 17.43%, CT-CP-REDV: 19.66%), (PL: 17.17%, PL-REDV: 24.00%, PL-CP-REDV: 20.87%), (NA: 14.94%, NA-REDV: 20.42%, NA-CP-REDV: 18.86%). And also confirmed by the O 1s spectra (Fig. 2b) at 531.3 eV where the signal of hydroxyls also overlaps with the amide group, O=C-N. The intensity of this signal increased for CT and NA functionalized samples, independently if they were physisorbed or silanized (CT: 49.89%, CT-REDV: 65.15%, CT-CP-REDV: 69.71%), (NA: 57.22%, NA-REDV: 61.63%, NA-CP-REDV: 59.81%) while PL treated surfaces did not detect an increase of this signal (PL: 88.42%, PL-REDV: 70.38%, PL-CP-REDV: 68.21%) since the effective activation process masks generated amides regarding hydroxyls groups.

3.1.4 Surface charge

Isoelectric point, IEP, and surface charge at pH=7.4 are given at Table 2. For all series, activated, silanized and functionalized, IEP is comprised between 3.5 and 4.7.

Changes between different surface modifications are relevant at pH 7.4. NaOH etching treated surfaces are the most negative surfaces at physiological pH while PL series is similar to control. The CPTES silane attachment to the surface is detected by a more negative surface charge for CT-CP, PL-CP and NA-CP. When REDV is physisorbed to the surface there is no statistically change of surface charge at physiological pH when comparing CT to CT-REDV, PL to PL-REDV and NA to NA-REDV. Contrary, ELR covalently attached to the surface is detected since surface charge is less negative compared to silanized series: CT-CP vs. CT-CP-REDV, PL-CP vs. PL-CP-REDV, NA-CP vs. NA-CP-REDV. This behaviour is specially accentuated for NA series since zeta potential changes from -34.9 mV for NA-CP to -26.7 mV for NA-CP-REDV, indicating a higher increment of ELR attached compared to CT-CP or PL-CP series.

3.2 ELRs biofunctionalized adlayer characterization

AFM images show REDV adsorbed adlayer morphology changes depending on the applied surface treatment (Fig. 3). REDV covered the entire surfaces but it tends to aggregate into a spherical morphology on all surfaces. Moreover, AFM analysis detected an increase of the mean roughness with the REDV coating, indicating a higher amount and thickness of the immobilized biomolecule adlayer with the increase of R_a. This effect is clear in silanized samples and, among them; NA-CP-REDV series obtained the higher R_a value.

Fig. 4 represents ΔD versus Δf plot for the adsorption process of ELR's on physisorbed and silanized CoCr sensors. The QCM-D technique allows quantifying the REDV attachment in real time without labelling fluorescent REDV. Nevertheless only CoCr coated sensors without any activation treatment, could be assayed. Thickness and surface mass density of the adlayer formed during experiments indicated that silanization considerably increases both parameters. Moreover CPTES silanization, CP-REDV, stiffens the attached REDV adlayer as observed by a decrease of the ΔD/Δf slope, compared to physisorbed series.

Finally, the stability of the FITC-REDV coating was determined after sonication during 1h in PBS 1X (Fig. 5). All surfaces lost a certain quantity of ELR after the procedure. Nevertheless, CPTES silanized series stated a higher amount of REDV after 1h sonication (PL-CP-REDV, NA-CP-REDV). NA-CP-REDV maintained the higher quantity over the surface compared to the other series after sonication. Non-functionalized samples, (C, PL, NA, PL-CP, NA-CP), did not present fluorescence.

3.3 Cell adhesion and proliferation

The response of HUVEC cells to the biofunctionalized surfaces was evaluated in vitro by means of early adhesion events (Fig. 6). After 4h of incubation, the presence of REDV elastin-like recombinamers slightly increased the total area occupied by cells attached onto CT surfaces. While the effect of REDV coating is slightly noticeable onto CT surfaces where cells were clearly round and a few of them spread; activated and/or activated and functionalized samples showed an increase of cell per surface area. When comparing surfaces activated and functionalized surfaces (and NA vs NA-REDV) it was observed that PL-CP, NA and NA-REDV presented the higher spreading, indicated by the higher index ratio and ø max parameters (Fig. 6b). But no differences in terms of cell spreading and number were observed between plasma activated and plasma functionalized surfaces (PL-CP vs PL-CP-REDV). However, it was a remarkable influence on the cell number and spreading behaviour of HUVEC cells on NaOH activated and functionalized surfaces specially compared CT.

Cells proliferated on the CT and NA-CP-REDV surfaces after 1 and 3 days in culture. After 1 day the number of cells was of CT: 3054.89 ± 202.66 cells/cm^2 and NA-CP-REDV: 4024.14 ± 720.76 cells/cm^2. Then, after 3 days in culture cells proliferated as follows CT: 4522.86 ± 697.85 cells/cm^2 and NA-CP-REDV: 4758.12 ± 793.02 cells/cm^2.

4. Discussion

The present study demonstrates the effectiveness of immobilizing REDV elastin-like-recombinamers on CoCr

surfaces to enhance endothelial cells adhesion and spreading. This approach could be used to enhance a rapid endothelialization of coronary stents. To overcome restenosis and obtain a functional artery after coronary stent implantation, it is decisive to accelerate stent surface endothelialization [7,11] and, if possible, without the use of antiproliferative drugs that generally delay the formation of healthy endothelium [8]. The elastin-like recombinamers used in this work contains the extracellular matrix protein sequence REDV from fibronectin and specific for the $\alpha_4\beta_1$ integrin receptor on human endothelial cells [19,38]. Therefore, the strategy reported in this work is an alternative to current coronary stents, which partially solve restenosis regardless recovery damaged tissue.

The designed ELR present alternatively along the chain, the (VPGKG) peptide unit which exhibits a primary amine that may serve for covalent immobilization through a nucleophilic attack [39] or aid for physisorption where it is induced weak bonding, i.e. dipole–dipole interactions, London dispersion forces and hydrogen bonding [39, 40].

A large number of metal surfaces, form a passivation layer of metal oxide that exposes hydroxyl groups on their surface, allowing the binding of silanes on the metal [41,42]. To ensure optimal silanization, several chemical and physical surface treatments are able to activate the metallic surface by increasing the amount of OH groups on the surface [43,44]. Oxygen plasma is known as an effective method for carbonaceous contamination removal without adding new particles on the surfaces [45,46]. On the other hand, sodium hydroxide etching has been widely used on titanium surfaces to induce surface bioactivity [47]. Oxygen plasma and NaOH etching were used as activation techniques on CoCr surfaces with different results.

Both activation treatments incremented the hydroxyl groups formation but PL treatment was the more efficient compared to NA and CT. Also confirmed by the O 1s peak deconvolution, Fig. 2b, the ratio OH^-/O^{2-} is higher for plasma treated samples compared to NA and CT. In addition, plasma process decreased the percentage of carbon and nitrogen and increased the amount of oxygen as a result of the removal contaminants; while NaOH etching activation slightly decreased carbon content and increased the amount oxygen and nitrogen. Then, NaOH treatment seems not to be so effective treatment in removing carbon species and to increase the formation of hydroxyls groups compared to oxygen plasma.

The activation treatments can also affect surface characteristics such as roughness, chemistry and changes in surface wettability or charge. As expected, activation with plasma treatment, PL series, didn't affect surface roughness. Moreover, plasma reduced the surface content of C and N resulting in a significant increase of surface wettability due to the contamination removal and the significant increase of hydroxyls on the surface. Otherwise, NaOH activation slightly increased surface nano-roughness, R_a=16.0 nm and hydrophobicity, compared to CT, due to the lower removal of carbonaceous species compared to plasma and also, due to the lower increase of the amount of hydroxyls groups on the surface.

The ζ potential, formally defined as the electrical potential at the electrokinetic slip plane, is a very important property of charged solid-liquid interfaces [48, 49]. The obtained zeta-potential curves showed a steadily more negative ζ potential as the solution increased alkalinity (data not shown). According to the results obtained, all tested surfaces are negatively-charged at physiological pH (7.4), particularly marked in NA samples. The charge formation process is due to the preferential adsorption of negatively-charged electrolyte anions, such as OH^-, Cl^-. The theoretical isoelectric point for REDV elastin-like recombinamer is around pH = 5.34 [50] then, at pH 7.4 the net charge is positive due to the amine groups of the polymer which tender to be progressively protonated with the increase of the pH. Therefore, surfaces with a less negative charge are expected to immobilize less REDV onto the surface at physiological pH since a lower difference in electronegativity between the surface and the biomolecules is detected.

Silanization has been widely used to covalently immobilize functional biomolecules on metallic supports [10,51] by being an alternative to physisorption process where weak bonds immobilize the cell adhesive molecules to the surface. CPTES silane bonds to -OH surface groups; then, it is expected that an augmentation of the mentioned bonds will increment the immobilized silane and, further, the ELR onto CoCr surfaces.

Silanization was confirmed by the detection of Si 2s and Cl 2p peaks unequivocally associated to CPTES molecules [43,52]. And a decrease of Co 2p and Cr 2p intensity peaks is detected, by XPS after silanization, which can be interpreted as the creation of a new layer over the surface. Although the detection of Cl 2p, and Si 2p over the surfaces is lower compared to other studies where CPTES silane has been attached to titanium, [52,53], the successful immobilization of ELRs and cell in vitro response to functionalized surfaces, corroborate the effectiveness of the proposed covalent immobilization strategy. The silanization process was further confirmed by the deconvolution of the O 1s peak of silanized but not functionalized samples (CT-CP, PL-CP, NA-CP) (data not shown) where 529.6 eV energy-bond corresponds to Si-O-Metal/Si-OH at 531 eV, and the Si-O-Si at 532.6 eV [50], detecting the presence of organ-silanes over the surfaces and then, demonstrating covalent bonding between the oxide metal and the CPTES silane.

The amount of immobilized REDV on the different surfaces is strongly influenced by the surface activation treatment which in turn produces changes in surface characteristics such as surface chemistry, roughness, charge, wettability and SFE [54,55]. Thus, functionalization of CoCr surfaces was thoroughly characterized by means of XPS, ζ potential, AFM, QCM-D and FITC-fluorescent labelling.

The surface chemical composition analysis of the present species by XPS corroborated the success of REDV immobilization through physisorption (CT-REDV, PL-REDV, NA-REDV) and CPTES silanization processes (CT-CP-REDV, PL-CP-REDV, NA-CP-REDV) by the increase in the percentage of C 1s and N 1s and a decrease in that of Co 2p and Cr 2p signals compared to activated (CT, PL, NA) and silanized series (CT-CP, PL-CP, NA-CP) (Table 1). Both effects are typically described for biomolecules attachment specially the presence of nitrogen corresponds to amide groups and amino functionalities characteristic of ELR sequences [56], whereas the immobilization of an ELR adlayer reduces the signal of cobalt and chromium oxides. The analysis of the O 1s spectra showed an increase of the second peak, 531.3 eV, assigned to carbonyl groups, especially amides, on functionalized surfaces compared to control (Fig. 2b). Statistically no differences were detected if functionalization is performed via covalent bonding or physisorption (CT-REDV: 65.15%, CT-CP-REDV: 69.71%, PL-REDV: 70.38%, PL-CP-REDV: 68.21%, NA-REDV: 61.63%, NA-CP-REDV: 59.81%) indicating that the silanization process is not optimal for immobilizing ELR onto CoCr surfaces. Moreover, no statistical differences were detected between different activation processes in the amount of amides groups by XPS. Probably the technique is not sensitive enough to distinguish between the detection of OH and O=C-N, other techniques should be used to determine the amount of REDV immobilized on the different surfaces.

QCM-D studies allowed to quantify the immobilized REDV but the experiments could only be performed on CoCr sensors with practically the same surface chemistry composition of CT surfaces (data not shown). Then, only physisorption and CPTES silanization processes were characterized in real time. Results, Fig. 4, demonstrated that functionalization with CPTES silane increases the amount and the thickness of immobilized REDV, 9.42 ng/mm^2, compared to physisorbed, 2.41 ng/mm^2. The frequency shift versus dissipation shift plot showed a single slope during REDV adsorption on CoCr sensors for both physisorbed and silanized series, indicating no conformational changes of the layer during adsorption. But, the slope value tends to zero indicating an increase of the rigidity of the biomolecules layer with the added mass for the silanized ELR series.

The conformation and the topography of the adsorbed REDV layer on the different CoCr surfaces were also visualized by AFM (Fig. 3). As observed, the changes in the mean roughness of the adsorbed layer were noticeable depending on the surface activation treatment, plasma or NaOH etching, and also the mechanism of immobilization, silanization or physisorption. The use of NaOH etching and CPTES silanization considerably increased the thickness of the REDV layer with a Ra (NA-CP-REDV) = 7.03 nm compared to physisorbed Ra (NA-REDV)= 4.57 nm or plasma activated Ra (PL-CP-REDV)= 2.63 nm. This result was further confirmed by ζ potential studies on functionalized samples. After REDV immobilization onto the surfaces, surfaces were less electronegative since REDV is positively charged at pH 7.4 (CT= -26.4 mV, CT-REDV= -25.3 mV, CT-CP-REDV: -24.7 mV). But it was

also observed that silanized and functionalized surfaces were less electronegative than physisorbed due to the higher immobilization of REDV onto the surface (NA = -31.1 mV, NA-REDV= -29.1 mV and NA-CP-REDV = -26.7 mV). Generally, the biomolecule did not adsorb homogeneously over the surfaces since it tends to agglomerate assuming a spherical shape. The reason of such shape can be related to the hydrophilic/hydrophobic behaviour of the ELR-coated surfaces. According to Costa et al [16], upon the formation of the spherical objects, it is plausible to assume that REDV present a more hydrophobic residue, which could result on an agglomerated coated surface. Then, the number of agglomerates is also an indication of the higher amount of immobilized biomolecules on the surface and then, depending on the applied surface treatment, it can increase or decrease. Again, NaOH etching and silanized surfaces are the ones with a higher ELR thickness and agglomerated ELR layer.

The characterization of the immobilized REDV adlayer was consistent since the determined thickness of physisorbed CT-REDV is about 2-2.5 nm, as seen by QCM-D and AFM, and a surface mass density of 2-2.41 ng/mm^2, as seen by QCM-D, these results were in accordance with other studies [57,58].

Finally, the stability of the immobilized biomolecule layer on the different surfaces was determined by quantifying the FITC-REDV intensity before and after sonication in PBS during 1 h (Fig. 5). As expected, after sonication, all samples decreased the signal intensity indicating that a certain quantity of FITC-REDV has been desorbed due to the process. A tendency was observed depending on the binding force between the biomolecule and the surface, silanized samples presented a major stability compared to physisorbed series but this effect was not statistically significant. The desorption on covalent attached samples could corroborate XPS previous results where probably not all the REDV immobilized on silanized surfaces was through covalent bonding, but a part of the immobilization was performed through physisorption. No relationship was found between the amount of hydroxyls activated on the surfaces and the amount of adsorbed biomolecule. Probably the reason is that, after the obtained XPS and stability results, the silanization process was not optimal to obtain all the biomolecules covalently attached onto the surface. Then, biomolecule adhesion is affected both by the immobilization process and surface electrostatic forces, where covalent bonding and a major difference in electronegativity between the surface and the biomolecule, lead to a higher REDV adsorption onto the treated CoCr surfaces [59,60].

The attachment of cells to metallic surface is strongly influenced by surface characteristics such as surface chemistry [60], roughness [62–64], charge and wettability [65,66] and SFE [67,68]. Our hypothesis is to immobilize engineered ELR with an REDV sequence specific for endothelial cells, expecting that a higher attachment of REDV onto CoCr surfaces will lead to a higher adhesion and spreading of HUVEC cells. HUVEC cell in vitro early adhesion studies showed differences depending on the surface activation and immobilization treatment and then, on the quantity of adsorbed biomolecules. In that sense, NaOH activated surfaces presented a major cell adhesion and spreading due to a higher amount of immobilized REDV onto the surface, also related with a higher electronegativity of the surface, -31.1 mV. Moreover, this surface significantly enhanced HUVEC proliferation in comparison to plain CoCr, with a higher number of cells at each time point. Plasma functionalized surfaces showed an increase of adhered cells compared to the control surface but inferior to NaOH functionalized series since a lower amount of REDV is immobilized. Moreover, no differences were observed in terms of cell adhesion parameters, between PL-CP and PL-REDV surfaces (Fig. 6b). This result indicates the great influence of surface charge in HUVEC cell adhesion since PL-CP surfaces were very electronegative at pH 7.4, -38.4 mV, thereby masking the effect of REDV coating onto PL activated surfaces. Contrary, on NA activated surfaces the effect of the immobilized REDV adlayer was more noticeable than surface charge properties. Taking together, both immobilization process and surface charge influenced the attached REDV layer where a higher amount is directly related to a higher HUVEC cell number and spreading response.

Conclusions

Elastin-like recombinamers functionalization of CoCr metallic surfaces for cardiovascular applications may offer an

efficient alternative to enhance rapid endothelialization. Herein, we have successfully immobilised REDV on the metallic surfaces through physisorption or covalent bonding by using traditional organosilane chemistry. The successful biomolecule adlayer was thoroughly quantified and characterized. Previously to functionalization, metallic surfaces were effectively activated to increase the amount of hydroxyls and then, enhancing silanization and, finally, improving ELR immobilization. Covalent bonding coatings of the ELR have shown higher amount and stability than the physisorbed ELR coatings. The results demonstrate that the silanization process was not completely effective since a mixture of covalent and physisorption behaviour was observed, the use of big biomolecules with different anchor groups causes covalent and weak bonding between the biomolecule and the surface. Both immobilization process and surface electrostatic forces influence the amount of immobilized ELR onto the surface. Most importantly, early HUVEC cell adhesion response was directly related to the amount of immobilized ELR on the surfaces. Thus, coating CoCr surfaces with REDV is a promising strategy to enhance rapid endothelialization and improve the long-term efficacy of cardiovascular stents.

Acknowledgments

Authors acknowledge the Spanish Government for financial support through project MAT 2012-30706, co-funded by the EU through European Regional Development Funds, and the Agency for Administration of University and Research Grants of the Government of Catalonia (2014 SGR 1333). We acknowledge financial support from the EU through the European regional development fund (ERDF), from the MINECO (MAT2013-41723-R y MAT2013-42473-R, PRI-PIBAR- 2011-1403, and MAT2012-38043), the JCyL (projects VA049A11, VA152A12, and VA155A12), the CIBER-BBN, the JCyL, and the Instituto de Salud Carlos III under the Network Center of Regenerative Medicine and Cellular Therapy of Castilla and Leon. M.I.C. would like to thank the Generalitat de Catalunya for funding through a FI Scholarship. The authors acknowledge Montse Dominguez and Romain Schieber for their useful technical assistance regarding the XPS and AFM analysis.

References

[1] J.C. Palmaz, Intravascular stents in the last and the next 10 years, J Endovasc Ther 11 Suppl (2004) 200–206.

[2] A. Tan, Y. Farhatnia, A. de Mel, J. Rajadas, M.S. Alavijeh, A.M. Seifalian, Inception to actualization: next generation coronary stent coatings incorporating nanotechnology, J. Biotechnol. 164 (2013) 151–70.

[3] R. Busch, A. Strohbach, S. Rethfeldt, S. Walz, M. Busch, S. Petersen, S. Felix, K. Stemberg, New stent surface materials: the impact of polymer-dependent interactions of human endothelial cells, smooth muscle cells, and platelets, Acta Biomater. 10 (2014) 688–700.

[4] P. Wenaweser, C. Rey, F.R. Eberli, M. Togni, D. Tüller, S. Locher, A. Remondino, C. Seiler, O.M. Hess, B. Meier, S. Windecker, Stent thrombosis following bare-metal stent implantation: success of emergency percutaneous coronary intervention and predictors of adverse outcome, Eur. Heart. J. 26 (2005) 1180–7.

[5] T. Simard, B. Hibbert, F.D. Ramirez, M. Froeschl, Y.-X. Chen, E.R. O'Brien, The evolution of coronary stents: a brief review, Can. J. Cardiol. 30 (2014) 35–45.

[6] F. Nazneen, G. Herzog, D.W. Arrigan, N. Caplice, P. Benvenuto, P. Galvin, M. Thompson, Surface chemical and physical modification in stent technology for the treatment of coronary artery disease, J. Biomed. Mater. Res. B Appl. Biomater. 100 (2012) 1989–2014.

[7] Y. Wei, Y. Ji, L.-L. Xiao, Q. Lin, J. Xu, K. Ren, J. Ji, Surface engineering of cardiovascular stent with endothelial cell selectivity for in vivo re-endothelialisation, Biomaterials 34 (2013) 2588–99.

[8] T. Inoue, K. Croce, T. Morooka, M. Sakuma, K. Node, D.I. Simon, Vascular inflammation and repair implications for re-endothelialization, restenosis, and stent thrombosis, JACC Cardiovasc. Interv. 4 (2011) 1057–66.

[9] L.G. Melo, M. Gnecchi, A.S. Pachori, D. Kong, K. Wang, X. Liu, R.E. Pratt, V.J. Dzau, Endothelium-targeted gene and cell-based therapies for cardiovascular disease, Arterioscler. Thromb. Vasc. Biol. 24 (2004) 1761–74.

[10] A. de Mel, G. Jell, M. Stevens, A. Seifalian, Biofunctionalization of biomaterials for accelerated in situ endothelialization: a review, Biomacromolecules 9 (2008) 2969–79.

[11] K. Zhang, T. Liu, J. Li, J. Chen, Surface modification of implanted cardiovascular metal stents: From antithrombosis and antirestenosis to endothelialization, J. Biomed. Mater. Res. A 102 (2014) 588–609.

[12] H. Chen, L. Yuan, W. Song, Z. Wu, D. Li, Biocompatible polymer materials: Role of protein–surface interactions, Prog. Polym. Sci. 33 (2008) 1059–87.

[13] M.H. Fittkau, P. Zilla, D. Bezuidenhout, M.P. Lutolf, P. Human, J.A. Hubbell, N. Davies, The selective modulation of endothelial cell mobility on RGD peptide containing surfaces by YIGSR peptides, Biomaterials 26 (2005) 167–74.

[14] D.F. Williams, The role of short synthetic adhesion peptides in regenerative medicine; the debate, Biomaterials 32 (2011) 4195–7.

[15] A. Girotti, A. Fernández□Colino. Elastin□like recombinamers: Biosynthetic strategies and biotechnological applications, Biotechnol. J. 6 (2011) 1174–86.

[16] R.R. Costa, C.A. Custódio, A.M. Testera, F.J. Arias, J.C. Rodríguez-Cabello, N.M. Alves, J.F. Mano, Stimuli-responsive thin Coatings Using Elastin-Like Polymers for Biomedical Applications, Adv Funct Mater 2009;19:3210–8.

[17] J.C. Rodríguez-Cabello, L. Martín, Emerging applications of multifunctional elastin-like recombinamers, Nanomedicine 6 (2011) 111–22.

[18] E. Monchaux, P. Vermette, Bioactive microarrays immobilized on low-fouling surfaces to study specific endothelial cell adhesion, Biomacromolecules 8 (2007) 3668–73.

[19] S.P. Massia, J.A. Hubbell, Vascular endothelial cell adhesion and spreading promoted by the peptide REDV of the IIICS region of plasma fibronectin is mediated by integrin alpha 4 beta 1, J. Biol. Chem. 267 (1992) 14019–26.
[20] H. Ceylan, A.B. Tekinay, M.O. Guler, Selective adhesion and growth of vascular endothelial cells on bioactive peptide nanofiber functionalized stainless steel surface, Biomaterials 32 (2011) 8797–805.
[21] D. Kereiakes, Usefulness of a cobalt chromium coronary stent alloy, Am. J. Cardiol. 92 (2003) 463–6.
[22] T. Hanawa, An overview of biofunctionalization of metals in Japan, J. R. Soc. Interface. 6 Suppl 3 (2009) S361–9.
[23] Y. Oshida, A. Hashem, T. Nishihara, M.V. Yapchulay, Fractal dimension analysis of mandibular bones: toward a morphological compatibility of implants, Biomed. Mater. Eng. 4 (1994) 397–407.
[24] B.C. Heng, P.P. Bezerra, Q.R. Meng, D.W. Chin, L.B. Koh, H. Li, H. Zhang, P.R. Preiser, F.Y. Boey, S.S. Venkatraman, Adhesion, proliferation, and gene expression profile of human umbilical vein endothelial cells cultured on bilayered polyelectrolyte coatings composed of glycosaminoglycans, Biointerphases 5 (2010) 53–62.
[25] A. Andukuri, W.P. Minor, M. Kushwaha, J.M. Anderson, H.-W. Jun, Effect of endothelium mimicking self-assembled nanomatrices on cell adhesion and spreading of human endothelial cells and smooth muscle cells, Nanomedicine 6 (2010) 289–97.
[26] S.J. Marshall, S.C. Bayne, R. Baier, A.P. Tomsia, G.W. Marshall, A review of adhesion science, Dent. Mater. 26 (2010) e11–6.
[27] A.W. Neumann, R.J. Good, C.J. Hope, M. Sejpal, An equation-of-state approach to determine surface tensions of low-energy solids from contact angles, J. Colloid. Interface Sci. 49 (1974) 291–304.
[28] A. Rudawska, E. Jacniacka, Analysis for determining surface free energy uncertainty by the Owen–Wendt method, Int. J. Adhes. Adhes. 29 (2009) 451–7.
[29] A.G. Hemmersam, M. Foss, J. Chevallier, F. Besenbacher, Adsorption of fibrinogen on tantalum oxide, titanium oxide and gold studied by the QCM-D technique. Colloids Surf. B Biointerfaces 43 (2005) 208-215.
[30] F. Höök, B. Kasemo, T. Nylander, C. Fant, K. Sott, H. Elwing, Variations in coupled water, viscoelastic properties, and film thickness of a Mefp-1 protein film during adsorption and cross-linking: a quartz crystal microbalance with dissipation monitoring, ellipsometry, and surface plasmon resonance study, Anal. Chem. 73 (2001) 5796–804.
[31] M.C. Biesinger, B.P. Payne, A.P. Grosvenor, L.W.M. Lau, A.R. Gerson, R.S.C. Smart, Resolving surface chemical states in XPS analysis of first row transition metals, oxides and hydroxides: Cr, Mn, Fe, Co and Ni, Appl. Surf. Sci. 257 (2011) 2717–30.
[32] B.V. Crist, A Review of XPS Data-Banks 1 (2007) 1–52.
[33] S. Surviliene, The use of XPS for study of the surface layers of Cr–Co alloy electrodeposited from Cr(III) formate–urea baths, Solid State Ionics 179 (2008) 222–7.
[34] G. Mani, M. Feldman, S. Oh, Surface modification of cobalt-chromium-tungsten-nickel alloy using octadecyltrichlorosilanes, Appl. Surf. Sci. 255 (2009) 5961–70.
[35] T. Hanawa, S. Hiromoto, K. Asami, Characterization of the surface oxide of a Co ± Cr ± Mo alloy after being located in quasi-biological environments using XPS, Appl. Surf. Sci. 183 (2001) 68–75.
[36] I. Milos, D. Du, P. Panjan, Chromium Nitride by XPS. Surf. Sci. 5 (1998) 138–44.
[37] I. Milošev, The effect of biomolecules on the behaviour of CoCrMo alloy in various simulated physiological solutions, Electrochim. Acta 78 (2012) 259–73.
[38] S. Liu, D.M. Rose, J. Han, M.H. Ginsberg, Alpha4 integrins in cardiovascular development and diseases, Trends Cardiovasc. Med. 10 (2000) 253–7.

[39] E. Salvagni, G. Berguig, E. Engel, J.C. Rodriguez-Cabello, G. Coullerez, M. Textor, J.A. Planell, F.J. Gil, C. Aparicio, A bioactive elastin-like recombinamer reduces unspecific protein adsorption and enhances cell response on titanium surfaces, Colloids Surf. B Biointerfaces 114 (2014) 225–33.

[40] Y.Noda, S. Noro, T. Akutagawa, T. Nakamura, Gold nanoparticle assemblies stabilized by bis(phthalocyaninato)lanthanide(III) complexes through van der Waals interactions. Scientific Reports 4 (2014) 3758.

[41] Y. Chen, X. Zheng, H. Ji, C. Ding, Effect of Ti–OH formation on bioactivity of vacuum plasma sprayed titanium coating after chemical treatment, Surf. Coatings Technol. 202 (2007) 494–8.

[42] H. Tamura, A. Tanaka, K. Mita, R. Furuichi, Surface Hydroxyl Site Densities on Metal Oxides as a Measure for the Ion-Exchange Capacity, J. Colloid. Interface. Sci. 209 (1999) 225–31.

[43] X. Chen, P. Sevilla, C. Aparicio, Surface biofunctionalization by covalent co-immobilization of oligopeptides, Colloids Surf. B Biointerfaces 107 (2013) 189–97.

[44] T. Hanawa, A comprehensive review of techniques for biofunctionalization of titanium, J. Periodontal Implant. Sci. 41 (2011) 263–72.

[45] V. Paredes, E. Salvagni, E. Rodriguez, Assessment and comparison of surface chemical composition and oxide layer modification upon two different activation methods on a CoCrMo alloy, J. Mater. Sci. Mater. Med. 43 (2013) 1–10.

[46] X. Liu, P. Chu, C. Ding, Surface modification of titanium, titanium alloys, and related materials for biomedical applications, Mater. Sci. Eng. R. Reports 47 (2004) 49–121.

[47] C. Aparicio, J.M. Manero, F. Conde, M. Pegueroles, J.A. Planell, M Vallet-Regí, F.J. Gil, Acceleration of apatite nucleation on microrough bioactive titanium for bone-replacing implants, J. Biomed. Mater. Res. Part A 82 (2007) 521–9.

[48] S.L. Walker, S. Bhattacharjee, E.M. V. Hoek., M. Elimelech, A novel asymmetric clamping cell for measuring streaming potential of flat surfaces, Langmuir 18 (2002) 2193–8.

[49] G.A. Parks, The isoelectric points of solid oxides, solid hydroxides, and aqueous hydroxo complex systems, Chem. Rev. 65 (1965) 177-198.

[50] L. Kozlowski, Calculation of protein isoelectric point (2012) Retrieved from http://isoelectric.ovh.org/.

[51] T. Hanawa, An overview of biofunctionalization of metals in Japan, J. R. Soc. Interface 6 Suppl. 3 (2009) S361–9.

[52] M. Godoy-Gallardo, C. Mas-Moruno, M.C. Fernández-Calderón, C. Pérez-Giraldo, J.M. Manero, F. Albericio, F.J. Gil, D. Rodríguez, Covalent immobilization of hLf1-11 peptide on a titanium surface reduces bacterial adhesion and biofilm formation, Acta Biomater. 10 (2014) 3522-34.

[53] M. González, E. Salvagni, J.C. Rodríguez-Cabello, E. Rupérez, F.J. Gil, J. Peña, J.M. Manero, A low elastic modulus Ti-Nb-Hf alloy bioactivated with an elastin-like protein-based polymer enhances osteoblast cell adhesion and spreading, J. Biomed. Mater. Res. A 101 (2013) 819–26.

[54] M. Pegueroles, C. Aparicio, M. Bosio, E. Engel, F.J. Gil, J.A. Planell, G. Altankov, Spatial organization of osteoblast fibronectin matrix on titanium surfaces: effects of roughness, chemical heterogeneity and surface energy, Acta Biomater. 6 (2010) 291–301.

[55] C.N. Elias, Y. Oshida, J.H.C. Lima, C.A. Muller, Relationship between surface properties (roughness, wettability and morphology) of titanium and dental implant removal torque, J. Mech. Behav. Biomed. Mater. 1 (2008) 234–42.

[56] A. Rezania, R. Johnson, A.R. Lefkow, K.E. Healy, Bioactivation of Metal Oxide Surfaces. 1. Surface Characterization and Cell Response, Langmuir 15 (1999) 6931–9.

[57] F. Höök, J. Vörös, M. Rodahl, R. Kurrat, A comparative study of protein adsorption on titanium oxide surfaces using in situ ellipsometry, optical waveguide lightmode spectroscopy, and quartz crystal microbalance/dissipation, Colloids Surfaces B 24 (2002) 155–70.

[58] Q. Lin, X. Ding, F. Qiu, X. Song, G. Fu, J. Ji, In situ endothelialization of intravascular stents coated with an anti-CD34 antibody functionalized heparin-collagen multilayer, Biomaterials 31 (2010) 4017–25.

[59] D.C. Hansen, Biological Interactions at metal surfaces, JOM 63 (2011) 22-23.

[60] J. Schneider, L.C. Ciacchi, A Classical Potential to Model the Adsorption of Biological Molecules on Oxidized Titanium Surfaces, J. Chem. Theory Comput. 7 (2011) 473–84.

[61] B.G. Keselowsky, D.M. Collard, A.J. García, Surface chemistry modulates focal adhesion composition and signaling through changes in integrin binding, Biomaterials 25 (2004) 5947–54.

[62] E. Potthoff, D. Franco, V. D'Alessandro, C. Starck, V. Falk, T. Zambelli, J.A. Vorholt, D. Poulikakos, A. Ferrari, Toward a rational design of surface textures promoting endothelialization, Nano. Lett. 14(2014) 1069–79.

[63] R. Barbucci, D. Pasqui, A. Wirsen, S. Affrossman, A. Curtis, C. Tetta, Micro and nano-structured surfaces, J. Mater. Sci. Mater. Med. 14 (2003) 721–5.

[64] S.J. Liliensiek, J.A. Wood, J. Yong, R. Auerbach, P.F. Nealey, C.J. Murphy, Modulation of human vascular endothelial cell behaviors by nanotopographic cues, Biomaterials 31 (2010) 5418–26.

[65] M. Pegueroles, F.J. Gil, J.A. Planell, C. Aparicio, The influence of blasting and sterilization on static and time-related wettability and surface-energy properties of titanium surfaces, Surf. Coatings Technol. 202 (2008) 3470–9.

[66] L. Ponsonnet, K. Reybier, N. Jaffrezic, V. Comte, C. Lagneau, M. Lissac, C. Martelet, Relationship between surface properties (roughness, wettability) of titanium and titanium alloys and cell behaviour, Mater Sci. Eng. C 23 (2003) 551–60.

[67] K. Cai, M. Frant, J. Bossert, G. Hildebrand, K. Liefeith, K.D. Jandt, Surface functionalized titanium thin films: zeta-potential, protein adsorption and cell proliferation, Colloids Surf. B Biointerfaces 50 (2006) 1–8.

[68] E.D. Kaufman, J. Belyea, M.C. Johnson, Z.M. Nicholson, J.L. Ricks, P.K. Shah, M. Bayless, T. Pettersson, Z. Feldoto, E. Blomberg, P. Claesson, S. Franzen, Probing protein adsorption onto mercaptoundecanoic acid stabilized gold nanoparticles and surfaces by quartz crystal microbalance and -potential measurements, Langmuir 23 (2007) 6053–62.

Figures Legends

Fig. 1. Wettability studies of activated and silanized CoCr surfaces: a) water contact angle. The * symbol indicates CA mean-values with non-statistically-significant differences respect to CT; b) surface free energy (SFE) and their different components (dispersive and polar). The #, *, & symbols join SFE and dispersive mean-values with non-statistically- significant differences. CT: polished CoCr. PL: polished CoCr treated with oxygen plasma. NA: polished CoCr, etched with NaOH. CT-CP: CT followed by CPTES silanization. PL-CP: PL followed by CPTES silanization. NA-CP: NA followed by CPTES silanization

Fig. 2. XPS high resolution spectra of C 1s (a) and O 1s (b) obtained at the modified CoCr surfaces after each reaction step. Polished CoCr samples (CT) were used as control. CT: polished CoCr. PL: polished CoCr treated with oxygen plasma. NA: polished CoCr, etched with NaOH. CT-REDV: CT with elastin-like recombinamer (ELR) (physisorbed). PL-REDV: PL with ELR (physisorbed). NA-REDV: NA with ELR (physisorbed). CT-CP-REDV: CT followed by CPTES silanization with ELR (covalent immobilization). PL-CP-REDV: PL followed by CPTES silanization with ELR (covalent immobilization. NA-CP-REDV: NA followed by CPTES silanization with ELR (covalent immobilization).

Fig. 3. AFM images and roughness parameters of ELR attachment on CoCr treated surfaces. Bar: 200 nm (for acronyms definition, see captions Fig.1 and Fig.2).

Fig. 4. ΔD versus Δf plot and adlayer parameters for the adsorption of RGD elastin-like polymer (500 μg/ml) on CoCr alloy coated sensors obtained by QCM-D. Calculations were performed after 4 h of adsorption time using the Voigt model. REDV: CoCr QCM-D sensor with ELR (physisorption). CP-REDV: CoCr QCM-D sensor followed by CPTES silanization with ELR (covalent immobilization).

Fig. 5. FITC-REDV stability test results on different treated CoCr surfaces before and after 1h of ultrasonic solicitations in PBS 1X at RT. Fluorescent measurement were performed after FITC ELR desorption with NaOH 0,2 M during 2h. The ¨, #, *, symbols join fluorescent intensities with non-statistically-significant differences (for acronyms definition, see captions Fig.1 and Fig.2).

Fig. 6. a) Fluorescent images of the HUVEC cells cultured for 4 h on CT, CT-REDV, PL-CP-REDV and NA-REDV surfaces in serum-free medium. Bars: 100 μm; b) quantification of the cell number, total area occupied by cells, aspect ratio and maximum diameter for the HUVEC cultured for 4 h on treated CoCr samples. Each area was analysed by FIJI ImageJ software was 869.7 μm × 689.07 μm (for acronyms definition, see captions Fig.1 and Fig.2).

Table 1

Table 1. XPS characterisation percentage of atomic composition at the different modified CoCr surfaces (for acronyms definition, see captions Fig.1 and Fig.2).

Surfaces	C 1s	O 1s	N 1s	Co 2p	Cr 2p	Ni 2p	W 4d	Cl 2p	Si 2s
CT	39.1 ± 2.0	37.7 ± 1.5	0.9 ± 0.3	9.0 ± 1.0	11.1 ± 0.1	1.0 ± 0.3	1.0 ± 0.0	0.0 ± 0.0	0.0 ± 0.0
PL	20.3 ± 0.2	54.3 ± 1.9	0.4 ± 0.1	15.2 ± 1.1	6.3 ± 1.0	2.5 ± 0.4	0.9 ± 0.1	0.0 ± 0.0	0.0 ± 0.0
NA	37.3 ± 5.8	42.4 ± 2.5	4.5 ± 0.1	6.7 ± 1.0	7.0 ± 0.5	0.8 ± 0.2	1.0 ± 0.7	0.0 ± 0.0	0.0 ± 0.0
CT-CP	31.3 ± 2.0	47.6 ± 0.8	0.5 ± 0.1	9.4 ± 1.0	7.7 ± 1.1	1.5 ± 0.5	0.7 ± 0.1	0.4 ± 0.1	0.9 ± 0.1
PL-CP	31.4 ± 3.1	44.6 ± 2.6	2.4 ± 1.3	9.0 ± 0.8	8.5 ± 1.1	1.7 ± 1.0	1.1 ± 0.4	0.4 ± 0.5	0.7 ± 0.5
NA-CP	28.0 ± 0.9	51.3 ± 2.6	0.3 ± 0.2	10.8 ± 1.0	5.3 ± 0.5	2.3 ± 0.6	0.9 ± 0.3	0.2 ± 0.2	0.8 ± 0.2
CT-REDV	52.0 ± 1.0	29.4 ± 1.5	8.6 ± 0.5	3.5 ± 0.3	4.9 ± 0.8	0.7 ± 0.0	0.8 ± 0.2	0.0 ± 0.0	0.0 ± 0.0
PL-REDV	55.8 ± 6.0	26.4 ± 4.1	12.4 ± 0.6	2.4 ± 1.3	2.1 ± 0.8	0.6 ± 0.2	0.4 ± 0.1	0.0 ± 0.0	0.0 ± 0.0
NA-REDV	50.1 ± 1.6	30.6 ± 0.7	9.0 ± 1.2	3.3 ± 0.2	5.3 ± 0.2	0.9 ± 0.1	0.7 ± 0.2	0.0 ± 0.0	0.0 ± 0.0
CT-CP-REDV	53.5 ± 2.6	27.6 ± 3.0	11.4 ± 1.0	2.2 ± 0.8	3.2 ± 0.6	0.4 ± 0.1	0.7 ± 0.1	0.2 ± 0.2	0.4 ± 0.1
PL-CP-REDV	52.1 ± 1.8	24.8 ± 1.1	11.7 ± 1.3	1.6 ± 0.4	2.4 ± 0.5	0.2 ± 0.0	0.5 ± 0.0	0.0 ± 0.0	0.6 ± 0.1
NA-CP-REDV	52.1 ± 1.8	30.3 ± 0.9	10.4 ± 0.4	2.0 ± 0.4	4.0 ± 0.3	0.2 ± 0.0	0.4 ± 0.0	0.1 ± 0.1	0.5 ± 0.4

Table 2

Table 2. Isoelectric point (IEP) and apparent zeta-potential (ζ), at pH 7.4, of modified CoCr surfaces (for acronyms definition, see captions Fig.1 and Fig.2).

Surfaces	IEP	ζ at pH = 7,4 (mV)
CT	3.5 ± 0.01	-26.4 ± 0.70
PL	3.8 ± 0.01	-27.1 ± 2.47
NA	4.1± 0.02	-31.1 ± 2.31
CT-CP	3.8 ± 0.01	-30.5 ± 4.38
PL-CP	3.7 ± 0.01	-38.4 ± 4.78
NA-CP	4.6 ± 0.01	-34.9 ± 3.61
CT-REDV	3.9 ± 0.00	-25.3 ± 2.63
PL-REDV	5.0 ± 0.04	-31.1 ± 0.54
NA-REDV	4.6 ± 0.04	-29.1 ± 4.19
CT-CP-REDV	4.7 ± 0.05	-24.7 ± 1.57
PL-CP-REDV	3.8 ± 0.00	-35.5 ± 5.35
NA-CP-REDV	4.5 ± 0.02	-26.7 ± 0.83

Fig. 1

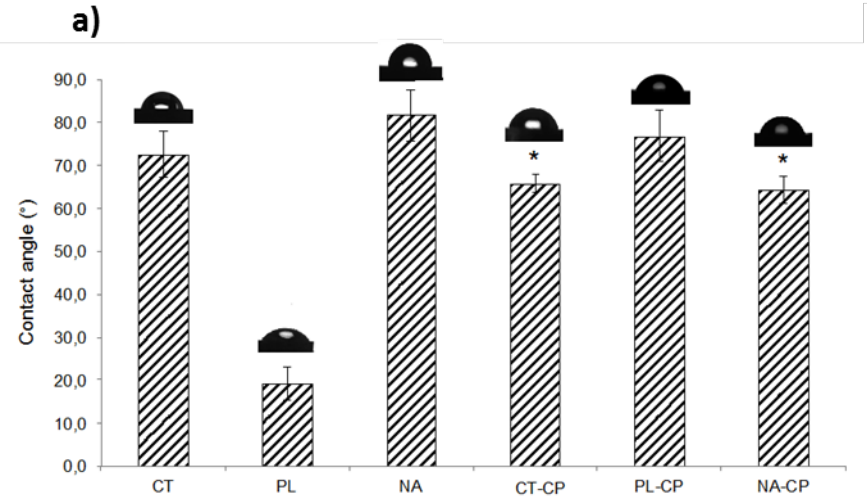
a)
Contact angle (°)
90,0
80,0
70,0
60,0
50,0
40,0
30,0
20,0
10,0
0,0
CT
PL
NA
CT-CP
PL-CP
NA-CP
*
*

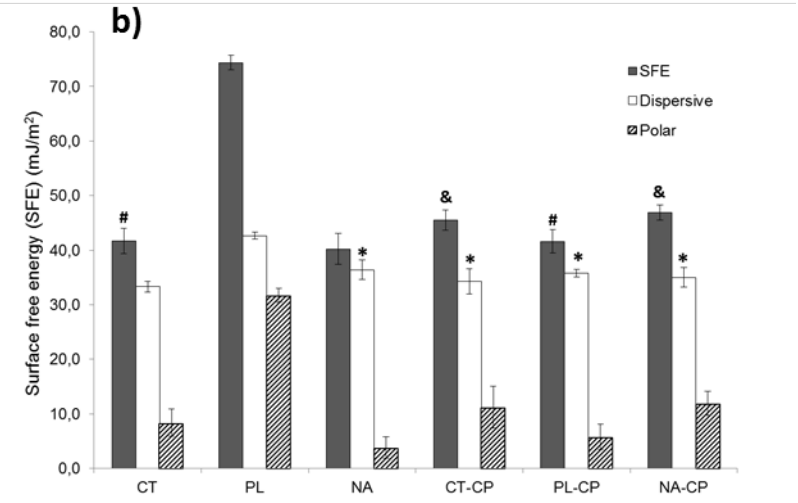
b)
Surface free energy (SFE) (mJ/m²)
80,0
70,0
60,0
50,0
40,0
30,0
20,0
10,0
0,0
SFE
Dispersive
Polar
#
&
*
CT
PL
NA
CT-CP
PL-CP
NA-CP

Fig.2

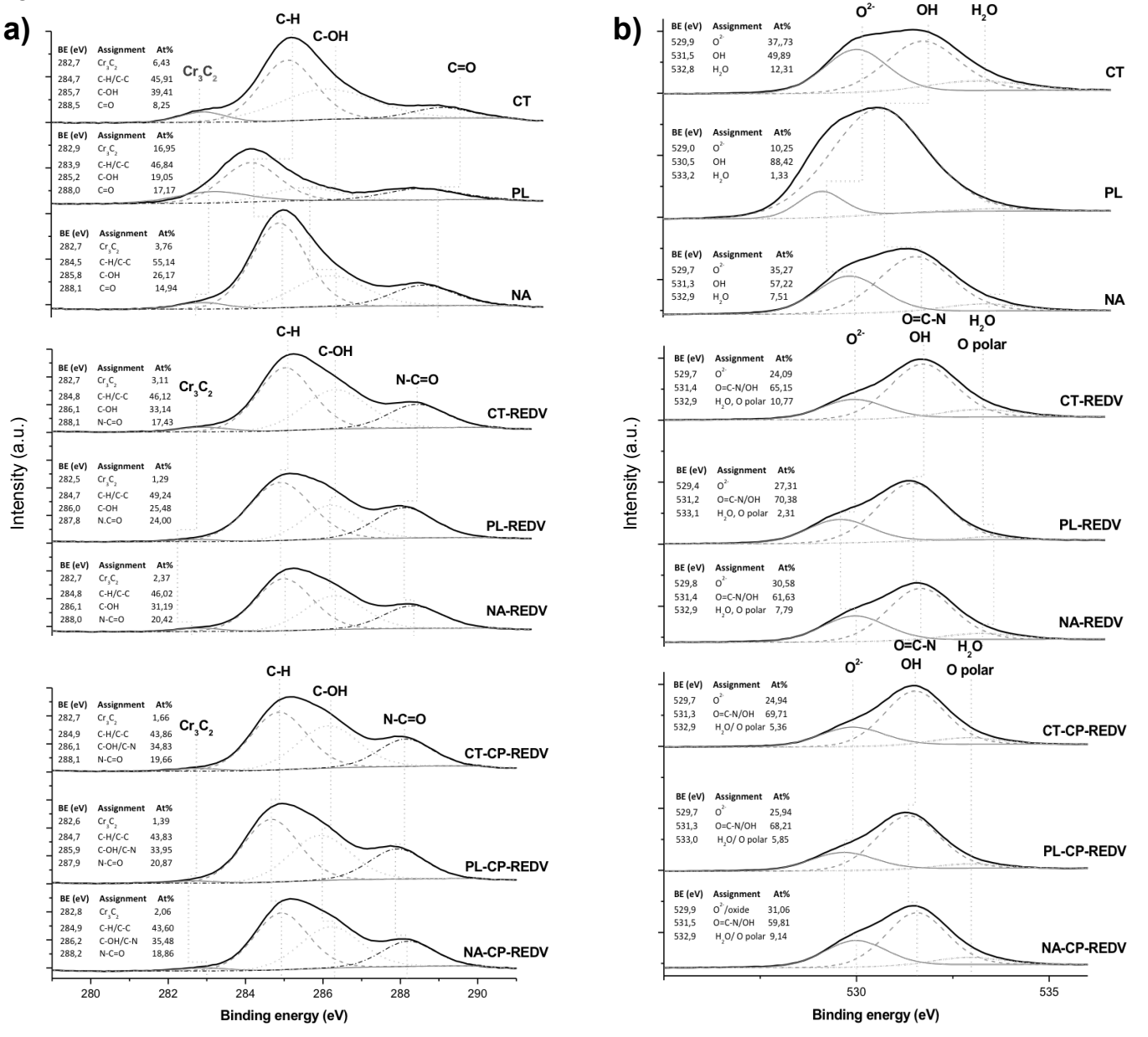
a)
C-H
C-OH
C=O
Cr3C2
BE (eV) Assignment At%
282,7 Cr3C2 6,43
284,7 C-H/C-C 45,91
285,7 C-OH 39,41
288,5 C=O 8,25
CT
BE (eV) Assignment At%
282,9 Cr3C2 16,95
283,9 C-H/C-C 46,84
285,2 C-OH 19,05
288,0 C=O 17,17
PL
BE (eV) Assignment At%
282,7 Cr3C2 3,76
284,5 C-H/C-C 55,14
285,8 C-OH 26,17
288,1 C=O 14,94
NA
C-H
C-OH
N-C=O
Cr3C2
BE (eV) Assignment At%
282,7 Cr3C2 3,11
284,8 C-H/C-C 46,12
286,1 C-OH 33,14
288,1 N-C=O 17,43
CT-REDV
BE (eV) Assignment At%
282,5 Cr3C2 1,29
284,7 C-H/C-C 49,24
286,0 C-OH 25,48
287,8 N.C=O 24,00
PL-REDV
BE (eV) Assignment At%
282,7 Cr3C2 2,37
284,8 C-H/C-C 46,02
286,1 C-OH 31,19
288,0 N-C=O 20,42
NA-REDV
C-H
C-OH
N-C=O
Cr3C2
BE (eV) Assignment At%
282,7 Cr3C2 1,66
284,9 C-H/C-C 43,86
286,1 C-OH/C-N 34,83
288,1 N-C=O 19,66
CT-CP-REDV
BE (eV) Assignment At%
282,6 Cr3C2 1,39
284,7 C-H/C-C 43,83
285,9 C-OH/C-N 33,95
287,9 N-C=O 20,87
PL-CP-REDV
BE (eV) Assignment At%
282,8 Cr3C2 2,06
284,9 C-H/C-C 43,60
286,2 C-OH/C-N 35,48
288,2 N-C=O 18,86
NA-CP-REDV
Intensity (a.u.)
280
282
284
286
288
290
Binding energy (eV)
b)
O2-
OH
H2O
BE (eV) Assignment At%
529,9 O2- 37,,73
531,5 OH 49,89
532,8 H2O 12,31
CT
BE (eV) Assignment At%
529,0 O2- 10,25
530,5 OH 88,42
533,2 H2O 1,33
PL
BE (eV) Assignment At%
529,7 O2- 35,27
531,3 OH 57,22
532,9 H2O 7,51
NA
O2-
O=C-N
OH
H2O
O polar
BE (eV) Assignment At%
529,7 O2- 24,09
531,4 O=C-N/OH 65,15
532,9 H2O, O polar 10,77
CT-REDV
BE (eV) Assignment At%
529,4 O2- 27,31
531,2 O=C-N/OH 70,38
533,1 H2O, O polar 2,31
PL-REDV
BE (eV) Assignment At%
529,8 O2- 30,58
531,4 O=C-N/OH 61,63
532,9 H2O, O polar 7,79
NA-REDV
O2-
O=C-N
OH
H2O
O polar
BE (eV) Assignment At%
529,7 O2- 24,94
531,3 O=C-N/OH 69,71
532,9 H2O/ O polar 5,36
CT-CP-REDV
BE (eV) Assignment At%
529,7 O2- 25,94
531,3 O=C-N/OH 68,21
533,0 H2O/ O polar 5,85
PL-CP-REDV
BE (eV) Assignment At%
529,9 O2-/oxide 31,06
531,5 O=C-N/OH 59,81
532,9 H2O/ O polar 9,14
NA-CP-REDV
Intensity (a.u.)
530
535
Binding energy (eV)

Fig. 3

a)

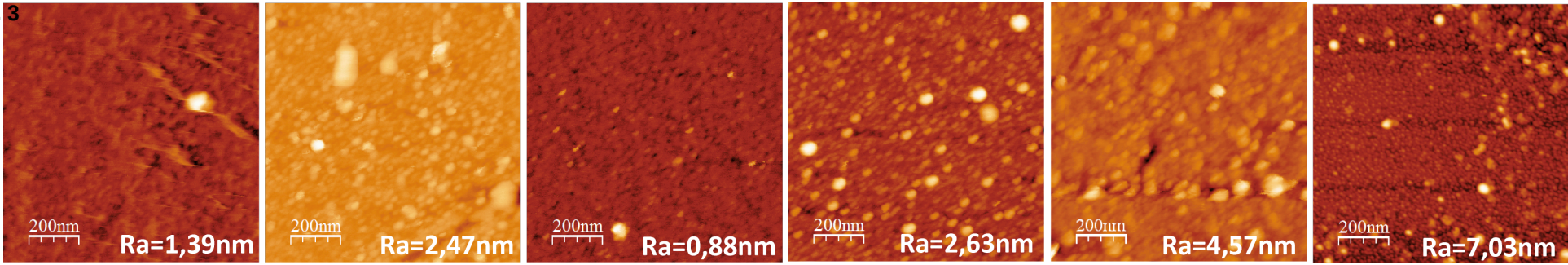
200nm
Ra=1,39nm
CT
200nm
Ra=2,47nm
CT-REDV
200nm
Ra=0,88nm
PL-REDV
200nm
Ra=2,63nm
PL-CP-REDV
200nm
Ra=4,57nm
NA-REDV
200nm
Ra=7,03nm
NA-CP-REDV

b)

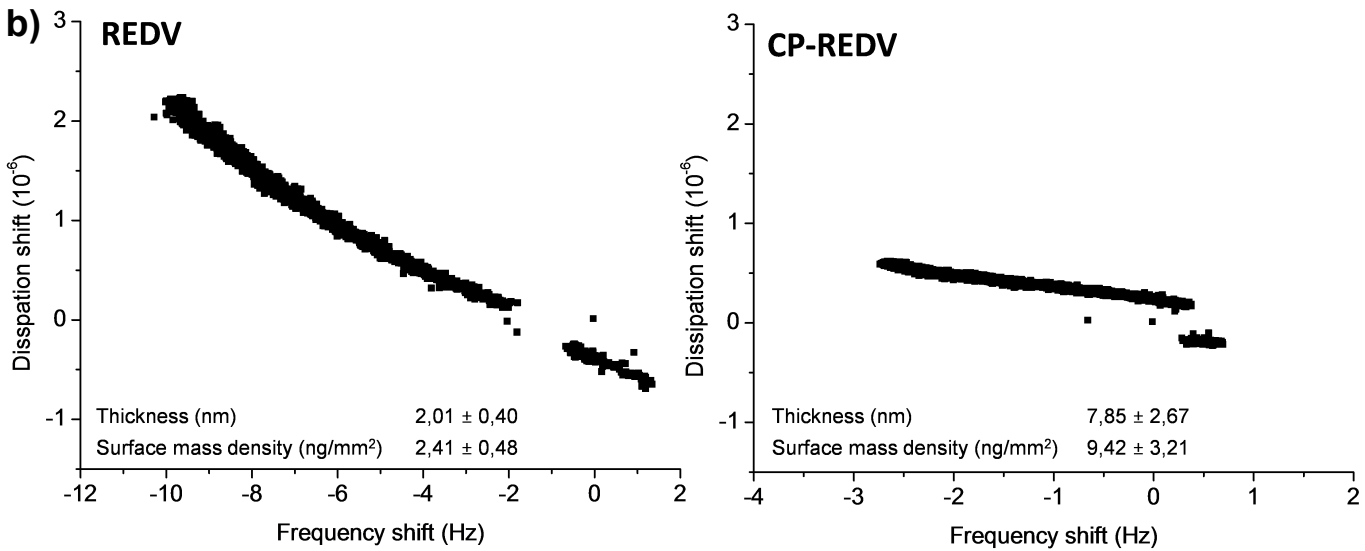
REDV
Dissipation shift (10-6)
Frequency shift (Hz)
Thickness (nm) 2,01 ± 0,40
Surface mass density (ng/mm2) 2,41 ± 0,48
CP-REDV
Dissipation shift (10-6)
Frequency shift (Hz)
Thickness (nm) 7,85 ± 2,67
Surface mass density (ng/mm2) 9,42 ± 3,21

Fig.4

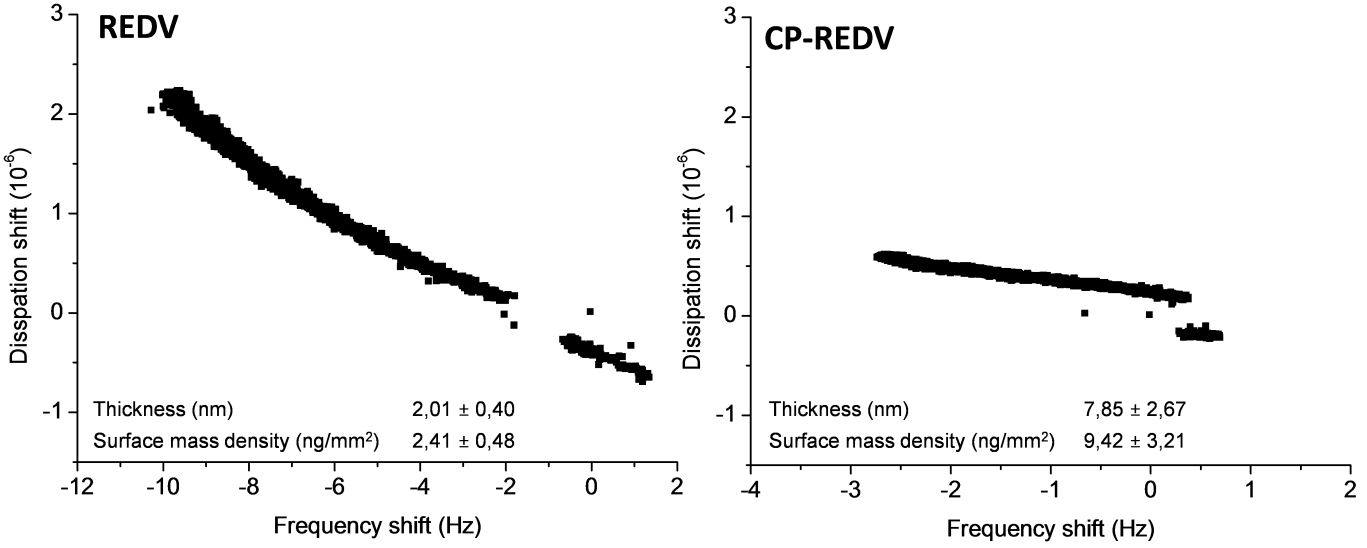
REDV
Dissipation shift (10-6)
Frequency shift (Hz)
Thickness (nm) 2,01 ± 0,40
Surface mass density (ng/mm2) 2,41 ± 0,48
CP-REDV
Dissipation shift (10-6)
Frequency shift (Hz)
Thickness (nm) 7,85 ± 2,67
Surface mass density (ng/mm2) 9,42 ± 3,21

Fig.5

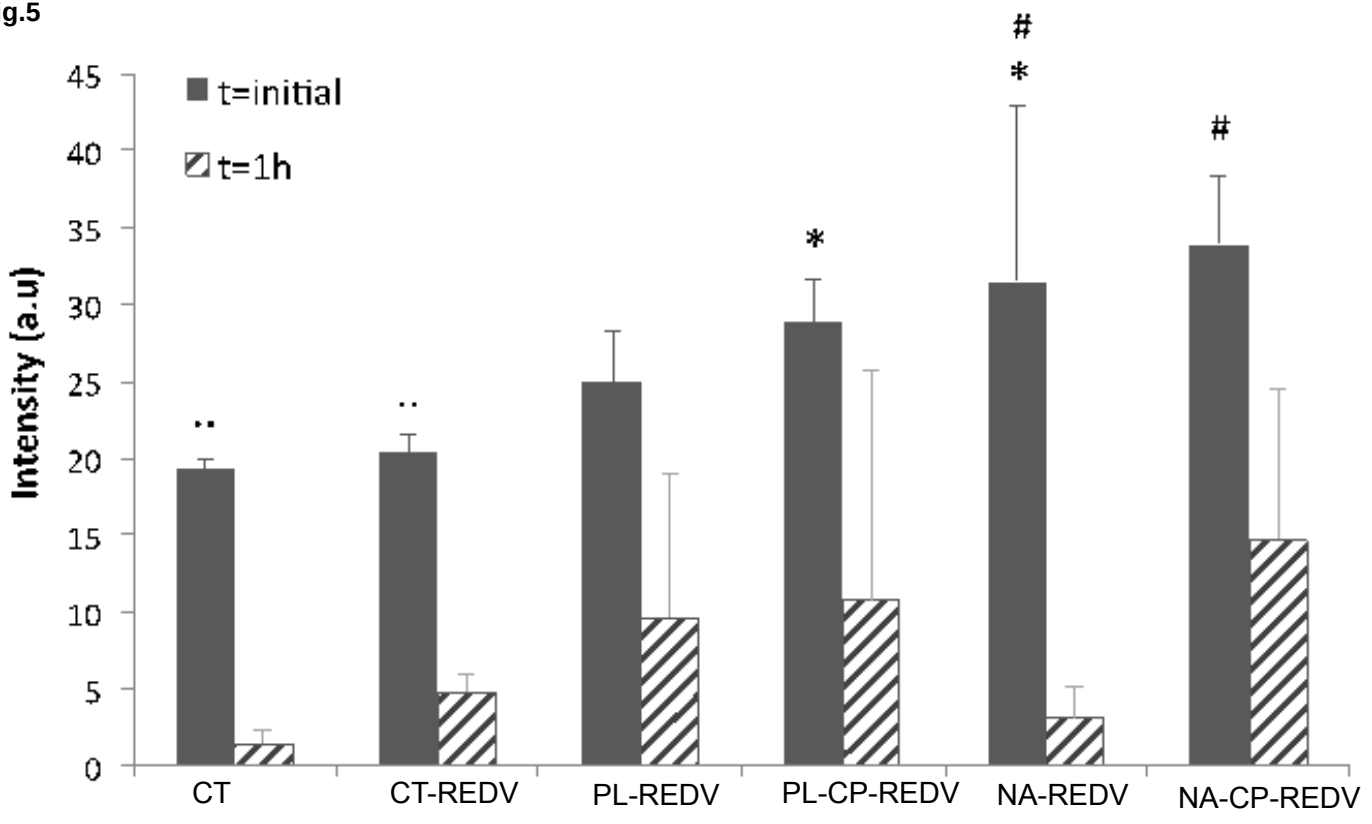
t=initial
t=1h
Intensity (a.u)
45
40
35
30
25
20
15
10
5
0
CT
CT-REDV
PL-REDV
PL-CP-REDV
NA-REDV
NA-CP-REDV

Fig. 6

a)

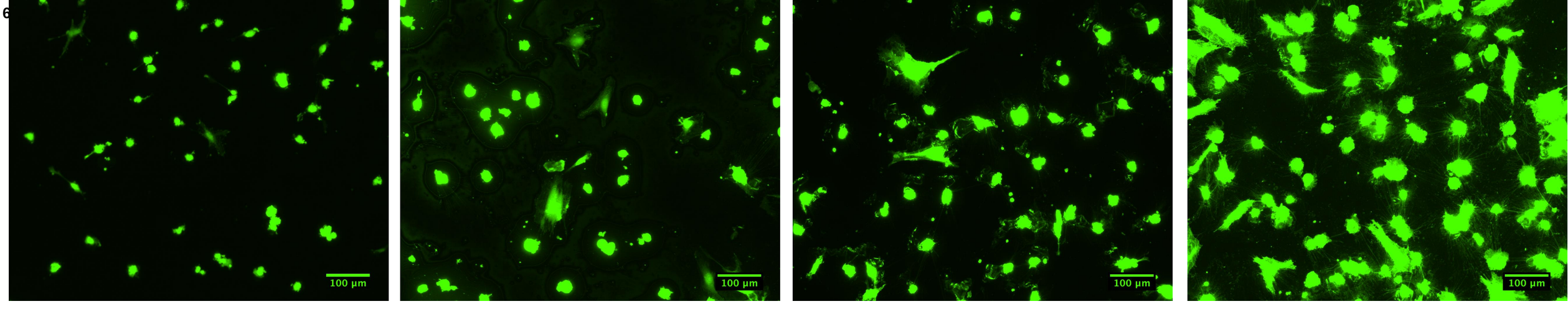

CT CT-REDV PL-CP-REDV NA-REDV

b)

Surfaces	Cells/cm^2	Total area occupied by cells (%)	Aspect Ratio	ø Max (µm)
CT	7634.1 ± 1626.4	17.5 ± 1.3	1.7 ± 0.7	40.2 ± 29.9
CT-REDV	7926.1 ± 1145.6	16.0 ± 0.7	1.7 ± 0.8	40.5 ± 22.9
PL-CP	6279.2 ± 1413.1	36.1 ± 2.1	1.9 ± 1.0	52.0 ± 20.8
PL-CP-REDV	7866.1 ± 1191.6	29.7 ± 1.6	1.6 ± 0.8	36.4 ± 18.3
NA	8698.7 ± 1932.5	31.6 ± 0.9	1.8 ± 0.9	49.7 ± 30.5
NA-REDV	9052.5 ± 1264.2	40.6 ± 1.2	1.7 ± 0.8	50.1 ± 30.8